THE JOURNAL OF BIOLOGICAL CHEMISTRY VOL. 288, NO. 24, pp. 17082–17090, June 14, 2013

Structural Diversity of Eukaryotic Membrane Cytochrome P450s*

Published, JBC Papers in Press, April 30, 2013, DOI 10.1074/jbc.R113.452805

Eric F. Johnson[‡1] **and C. David Stout**[§]

From the Departments of [‡]*Molecular and Experimental Medicine and* [§]*Integrative Structural and Computational Biology, The Scripps Research Institute, La Jolla, California 92037*

X-ray crystal structures are available for 29 eukaryotic microsomal, chloroplast, or mitochondrial cytochrome P450s, including two non-monooxygenase P450s. These structures provide a basis for understanding structure-function relations that underlie their distinct catalytic activities. Moreover, structural plasticity has been characterized for individual P450s that aids in understanding substrate binding in P450s that mediate drug clearance.

Structural characterization of eukaryotic membrane cytochrome P450s has focused largely on human cytochrome P450s because of their importance in human health. Human P450s are either specialists that exhibit highly conserved functions in vertebrate species or generalists that facilitate metabolic clearance of structurally diverse compounds to reduce toxic exposures, although in some cases, mutagenic or more toxic metabolites are produced. Genes encoding generalist P450s vary between closely related species, leading to functionally distinct enzymes (1, 2). P450s are identified by a family number, subfamily letter, and either a shared number for orthologs in different species or a unique number for paralogs. Family and subfamily designations reflect >35% and >70% amino acid sequence identity, respectively. Orthologs typically exhibit 70% or greater sequence identity. There are 57 genes encoding human P450s comprising 18 families, including 35 genes for predominantly generalist P450s in families 1–4.

Common Features of Membrane P450 Structures

The catalytic domain of ~460 amino acids folds into a triangular prism shape (Fig. 1*A*) that is similar to that of soluble prokaryotic P450s (3). Twelve α-helices first identified for the structure of soluble prokaryotic 101A1 (4) are designated by letters A–L. Additionally, there is a highly conserved β-sheet domain near the N terminus of the protein. The number of helices is typically larger, but these helices are less conserved (Fig. 1). Spatial conservation is highest for the structural core of the protein and diverges most for the substrate-binding site (5, 6).

The heme prosthetic group is the catalytic center of the enzyme, where a reactive hypervalent oxo-iron protoporphyrin IX radical cation intermediate is formed for subsequent insertion of the iron-bound oxygen atom into a substrate bond (7). Substrates bind in a cavity or cleft above the surface of the heme in proximity to the reactive intermediate (Fig. 1). The thiolate side chain of a conserved cysteine binds to the axial coordination site of the iron opposite to the bound oxygen, giving rise to the unique spectral and functional properties of P450 enzymes.

Most P450s are monooxygenases, and electrons for reduction of the heme and subsequently the oxygen substrate are provided by protein partners that bind to the face of the protein proximal to the heme (8–11). Reduced adrenodoxin (12), a soluble Fe-S protein, serves as the reductant for vertebrate mitochondrial P450s, and in turn, it is reduced by the flavoprotein NADPH-adrenodoxin oxidoreductase. A structure of mitochondrial 11A1 crystallized with a tethered adrenodoxin bound to its proximal surface reveals the binding interaction between the proteins (10). Microsomal NADPH-cytochrome P450 oxidoreductase, which has an FMN and an FAD domain, provides two electrons for reduction of oxygen by microsomal P450s. The microsomal reductase has been crystallized in a closed form in which the flavodoxin-like FMN domain is positioned for reduction by the FAD domain (13) and in a more open form in which the FMN domain is more accessible for interaction with the proximal face of the P450 (8, 14, 15). Microsomal cytochrome b_5 can also serve as a donor of the second electron, and interactions between cytochrome b_5 and P450s can modulate rates and product profiles (16).

Helices C, D, and I–L, together with β-sheets 1 and 2, comprise the structural core that forms portions of the heme-binding site and the proximal surface where protein partners bind. Helix F-G, helix B-C, and the N- and C-terminal regions, which form the outer boundaries of the substrate-binding cavity, are more dynamic and exhibit more varied secondary and tertiary structures (Fig. 1). The flexibility of this architecture was first demonstrated for P450 102A1, which exhibited an open channel to the active site when crystallized without a substrate (17) and a closed form when a substrate was bound (18). Several solvent access channels (Fig. 2) that can expand, contract, and merge for substrate access and product exit have been defined from structures and molecular dynamics studies (19).

Membrane Binding

Microsomal P450s are targeted to the endoplasmic reticulum by an N-terminal leader that includes a transmembrane helix (Fig. 2) that is linked by a polar connector to the catalytic domain, which is sequestered to the cytoplasmic side of the membrane (20). With the exception of 19A1 (21), microsomal P450s have been expressed for structure determinations without their N-terminal leader sequences, as described initially for rabbit microsomal 2C5 (3, 22). The hydrophobic surfaces of helices A′, F′, and G′ of microsomal P450s provide additional interactions with the membrane surface (3, 22–25). Helices F′ and G′ are not typically seen in prokaryotic P450s, and they are formed by a longer polypeptide chain connecting helices F and G in eukaryotic membrane P450s. Helix F′ resides between

* This work was supported, in whole or in part, by National Institutes of Health Grant R01 GM031001 from NIGMS. This is the third article in the Thematic Minireview Series on Cytochrome P450.

[1] To whom correspondence should be addressed. E-mail: johnson@scripps.edu.

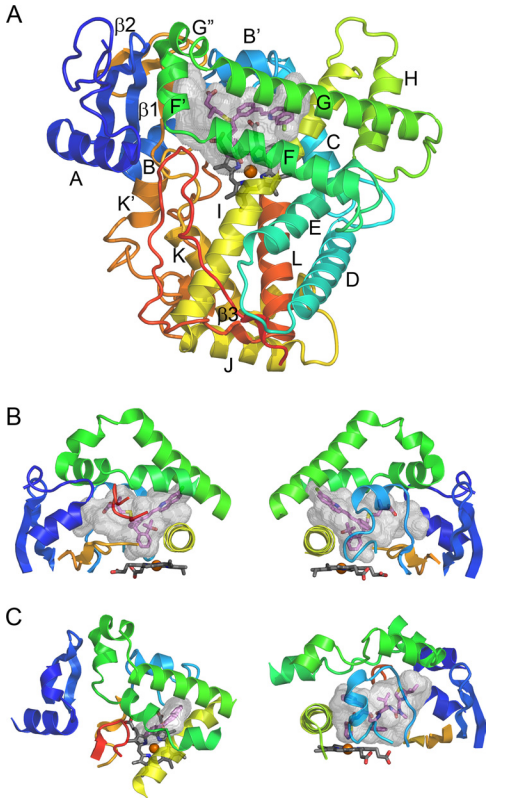

FIGURE 1. **P450 fold and elements comprising the active site.** *A*, the overall topology is illustrated by the structure of microsomal 2C8 (Protein Data Bank code 2NNI), colored from *blue* at the N terminus to *red* at the C terminus. The active site cavity is shown as a *transparent* surface. The bound substrate, montelukast (*violet* carbons), and the heme prosthetic group (*gray* carbons) are shown as *stick* figures. Twelve helices designated by letters and β-sheets 1 and 2 are highly conserved. Additional helices that are named by letters with primes or double primes are evident. *B*, two views of structural components that form the sides of the substrate-binding site of 2C8. The helix F-G region (*green*) forms the top of the cavity and is cantilevered over helix I (*yellow*), which forms one side. The opposite side is formed by connections (*orange*) between helix K and β-strands 1–3 and between β-strands 1–4 and helix K′ near the surface of the heme and by the N-terminal region (*dark blue*) that includes helix A and β-strand 1. The gaps under the helix F-G region between helix I and the N-terminal region are filled by the C-terminal loop (*red orange*) as shown in the *left panel* and by the B-C loop (*light blue*) as shown in the *right panel*. *C*, views of the helix F-G side of the microsomal 1A2 complex with α-naphthoflavone (*left*) and of the B-C loop side of the microsomal 3A4 complex with ritonavir (*right*) illustrate differences in the topologies of the active sites and the secondary and tertiary structures of 2C8 (code 2NNI), 1A2 (code 2HI4), and 3A4 (code 3NXU).

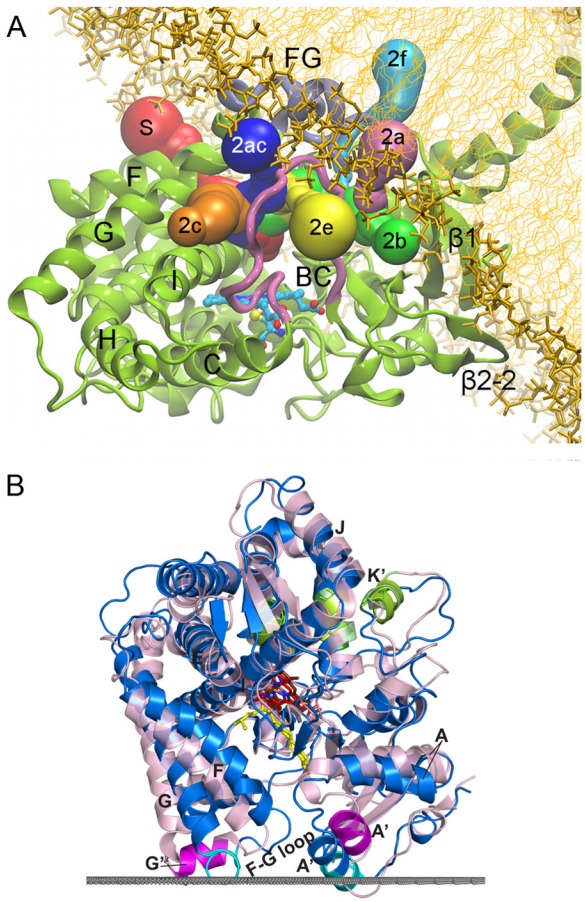

FIGURE 2. **Interactions of microsomal (*A*) and mitochondrial (*B*) P450s with the membrane.** *A*, Fig. 5*A* from Cojocaru *et al.* (32) reproduced here under the terms of the Creative Commons Attribution License. A model of microsomal 2C9 (*ribbon*) embedded in a 1-palmitoyl-2-oleoylphosphatidylcholine bilayer (*thick* and *thin gold sticks*) is depicted. The colored tubes represent solvent access channels that were observed to open and, in some cases, close during molecular dynamics simulations and are labeled according to the nomenclature of Cojocaru *et al.* (19). The region between helices F and G is designated *FG*. *B*, Fig. S6 from Mast *et al.* (33). Structures of 11A1 (*blue*; Protein Data Bank code 3MZS) and 24A1 (*pink*; code 3K9V) are shown. The upper surface of the membrane bilayer with respect to 11A1 is indicated by the *gray line*. The membrane insertion sequences are colored *cyan* in 11A1 and *magenta* in 24A1. Secondary structural elements that participate in adrenodoxin binding are colored *green*. 22-Hydroxycholesterol is shown in *yellow*; heme is shown in *red* in 11A1 and *brown* in 24A1.

β-sheet 1 and the helix B-C loop and above a heme propionate. In membrane P450s, this heme propionate is usually positioned below the plane of the heme, which increases space below helix F′, whereas in soluble prokaryotic P450s, this propionate typically resides above the plane (26). The leader sequences targeting family 11, 24, and 27 P450s to mitochondria are cleaved upon import (27, 28), and membrane binding to the matrix side of the inner membrane is likely to reflect interactions of the hydrophobic external surfaces of helices A′ and G′ with the membrane (Fig. 2) (29, 30).

Interactions of helices A′, F′, and G′ with the membrane suggest that some substrate access channels are likely to open into the membrane, whereas those that open on sides of the active site and under the helix F-G region will open to the cytosol (Fig. 2). Molecular dynamics studies of microsomal 2C9 (31, 32) and 3A4 (26) in solution and bound to phospholipid bilayers indicate that the opening and closing of solvent channels can be modulated by such interactions compared with simulations in a homogeneous aqueous medium.

Specialist Enzymes

Mitochondrial enzymes are specialists that generate specific products that fulfill their physiologic functions. Mitochondrial 11A1 catalyzes the first step in steroid hormone synthesis by successive oxygenations that result in scission of the C21–C22 bond of cholesterol to form pregnenolone and isocaproaldehyde. Structures of 11A1 co-crystallized with cholesterol and with the two intermediate products, (22*R*)-hydroxycholesterol (Fig. 2*B*) and (22*R*,20*R*)-dihydroxycholesterol, bound in the active site (10) indicate that the sterol ring system is positioned under helix F′, with the side chain positioned with C22 and C20 in close proximity to the heme iron for each substrate. A struc-

ture determined for the bovine 11A1 (22*R*)-hydroxycholesterol complex (33) indicates that this substrate-binding site is highly conserved. Mitochondrial 24A1 catalyzes a similar reaction that cleaves the side chain of calcitriol to inactivate the hormone. A structure of rat mitochondrial 24A1 crystallized in the absence of its substrate exhibits an open substrate-binding cleft between helices A′ and F′, and when calcitriol binds, the cleft is likely to close and resemble structures of 11A1 (Fig. 2*B*) (30). Cholesterol 3-sulfate binds in a similar way in a structure of microsomal 46A1, with the side chain positioned for hydroxylation of C24. This is an important reaction for the clearance of excess cholesterol from the brain. Interestingly, the substrate-free structure of 46A1 exhibits a much different cavity shape (34), and the 46A1 active site adapts to bind several structurally unrelated inhibitors (35, 36). In contrast, structures of microsomal 2R1 (37) indicate that the secosterol moiety of vitamin D_3 and related compounds is bound between helices I and G and the helix B-C loop. This positions the side chain for 25-hydroxylation, which is the first step in the conversion of vitamin D_3 to calcitriol.

The sterol ring system is positioned much differently in a structure of microsomal 7A1 (Protein Data Bank code 3SN5), where cholest-4-en-3-one resides above the heme propionate side chains, with the plane of the sterol rings parallel to the heme plane. The site of metabolism, C7, is positioned closest to the heme iron. Hydroxylation at C7 is the rate-limiting step in bile acid formation from cholesterol. Similarly, a structure of the human aromatase, microsomal 19A1, crystallized with androstenedione (21) indicates that the long axis of the steroid is almost parallel to the heme plane, with the 19-methyl group positioned for reaction with the reactive intermediate. Estrogens are formed by three successive oxygenations at C19, which leads to elimination of formic acid and to aromatization of ring A (38). A structure of 19A1 complexed with exemestane, an inhibitor used clinically to reduce estrogen formation in breast cancer patients, led to the synthesis of new inhibitors with increased potency (39).

Similarly, inhibitors of microsomal 17A1 are used to inhibit androgen formation to treat prostate cancer. The first step of androgen biosynthesis is 17α-hydroxylation of pregnenolone, which is followed by a second oxygenation that results in scission of the C17–C20 bond to produce androstenedione and acetic acid. Structures of 17A1 were determined with a Food and Drug Administration-approved first-in-class inhibitor (abiraterone) and with another inhibitor (TOK-001) that is in clinical trials (40). In this case, the long axis of the inhibitors is almost perpendicular to the plane of the heme (40). A similar orientation was observed for 17α-hydroxyprogesterone in a structure of 21A2 (41). Microsomal 21A2 catalyzes the 21-hydroxylation of 17α-progesterone and progesterone to form precursors for the synthesis of cortisol by 11B1 and aldosterone by 11B2, respectively. The binding of deoxycorticosterone to mitochondrial 11B2 is similar to that of androstenedione in 19A1, but with C11 and the 18-methyl group placed near the heme iron (42).

Interestingly, human microsomal 51A1 is an anti-target for development of therapeutic inhibitors that target 51A1 in fungal pathogens. Human 51A catalyzes the 14α-demethylation of lanosterol, another carbon–carbon bond scission reaction, in the pathway for *de novo* synthesis of cholesterol. It is anticipated that the availability of structures for human 51A1 (43) and 51A1 orthologs in fungal pathogens (44–46) will aid in the design of drugs that are more selective for fungal 51A relative to the human enzyme.

Isomerases and Other Non-monooxygenases

Humans express two specialist microsomal P450s (8A1 and 5A1) that catalyze the isomerization of prostaglandin H_1 to produce prostacyclin and thromboxane, respectively. Structures of human (47) and zebrafish (48) 8A1 in the ligand-free state have been determined, and conserved characteristics of the active site architectures were noted (48). U51605, a substrate analog with nitrogens substituted for the endoperoxide oxygens, binds with the C11 nitrogen coordinated to the heme iron (48). This is consistent with the proposed initial binding of the C11 oxygen of the endoperoxide moiety to the heme iron to initiate the isomerase reaction (49). The C9 nitrogen exhibits a hydrogen bond with the side chain of Asn-277 on helix I of 8A1 (48). This asparagine is conserved in plant non-monooxygenases of the CYP74 family, such as chloroplast allene oxide synthase, in which the corresponding asparagine is thought to facilitate conversion of lipid peroxides to allene oxides (50). These studies also noted that alterations in the proximal surface would likely prevent interactions with electron donors for P450 monooxygenases (48, 50).

Carcinogen-metabolizing Enzymes

Each generalist P450 transforms a wide range of lipophilic substrates to more polar compounds to enhance elimination. Unfortunately, P450s can also transform procarcinogens to direct acting mutagens. Six microsomal P450s (1A1, 1A2, 1B1, 2E1, 3A4, and 2A6) account for >90% of known carcinogen activation pathways (51). Structures of 1A1 (Protein Data Bank code 4I8V), 1A2 (52), and 1B1 (53) co-crystallized with the inhibitor α-naphthoflavone (272 Da) indicate that their active sites are narrow, with large hydrophobic surfaces suitable for binding polynuclear aromatic hydrocarbons (Fig. 1). A bend in helix F reinforces the narrow cavities. Interestingly, amino acid residues that line these cavities are conserved in other species, which is likely to reflect persistent environmental exposure to these compounds during evolution. In contrast, sequence conservation is much less evident for portions of the polypeptide chains that form the active site surfaces of family 2 P450s. This was first predicted from sequence alignments with the primary and tertiary structures of bacterial 101A1 (54) and confirmed by structure determinations.

The active site cavity of the principal enzyme for nicotine clearance (2A6) co-crystallized with coumarin (146 Da) (55), with nicotine (162 Da) (56), and with several inhibitors (55, 57) is smaller than that of family 1 P450s. Relatively small differences in rotamer and backbone conformations are evident for these complexes. A somewhat larger and more plastic active site relative to 2A6 is evident for 2A13, which ultimately converts nicotine and cotinine to carcinogenic nitrosamines such

as nicotine-derived nitrosamine ketone (NNK[2]; 4-(methylnitrosamino)-1-(3-pyridyl)-1-butanone) in lung tissues (56, 58).

Microsomal 2E1 co-crystallized with indazole (118 Da) and 4-methylpyrazole (82 Da) exhibits the smallest cavity (59). The active site expands when C_8, C_{10}, and C_{12} fatty acids with an azole ring attached to the terminal carbon are bound. The azole group coordinates to the heme and positions the terminal aliphatic carbon of the fatty acid constituent to mimic the position for ω-hydroxylation. A minor shift in the position of Phe-298 on helix I allows the carboxylate moieties to reside in an adjacent cavity between helices I, F, and G and increases the volume of the active site from ~190 Å^3 for indazole to 420–490 Å^3 for the C_8–C_{12} compounds (60). Structures of 2E1, 2A6, and 2A13 co-crystallized with pilocarpine reveal conformational changes and differences in binding interactions (61).

Drug-metabolizing Enzymes

Drug clearance pathways mediated by P450s can be a formidable barrier to the development of orally available new drugs. Structures of drug-metabolizing P450s can be used to improve predictions of sites of metabolism and provide information for drug redesign to overcome metabolic barriers to improve efficacy or to reduce the likelihood of drug-drug interactions (62–65). Hepatic clearance of drugs by P450-mediated metabolism is the most prevalent pathway for elimination of the 200 most prescribed drugs and is attributed in order of frequency to microsomal P450s 3A4, 2C9, 2D6, 2C19, 1A2, 2C8, and 2B6 (66). With the exception of 2B6, structures of these enzymes exhibit active site cavities that are larger than that of 1A2 and that are more open and pliant.

3A4 structures differ from family 1 and 2 structures because helices F and G do not extend across the active site cavity (Fig. 1). In 3A4, the "roof" above the heme is formed by a cluster of phenylalanine side chains. These phenylalanine side chains expand outward relative to the ligand-free structure (67, 68) to accommodate erythromycin (734 Da) (69), ritonavir (721 Da) (70), desthiazolylmethyloxycarbonyl ritonavir (580 Da) (71), or two molecules of ketoconazole (531 Da) stacked antiparallel and vertically above the heme (69). In contrast, bromoergocryptine (656 Da) elicits only small changes relative to ligand-free structures when bound (72). Co-crystallization of progesterone with 3A4 identified a peripheral binding site for the steroid near the outer surface of helices F′ and G′ and the phenylalanine cluster (68). 3A4 often exhibits homo- and heterotropic activation kinetics with progesterone and other substrates of similar size that are consistent with the binding of two or more molecules to the enzyme (73, 74). Biophysical studies have suggested that two molecules can stack in the active site (75), as seen for the 3A4 structure with two molecules of ketoconazole (69), and have provided evidence for a peripheral binding site such as that observed for progesterone (76).

The active site cavity of 2C8 is large but has a more serpentine shape than that of 3A4 (Fig. 1). The cavity readily accommodates montelukast (586 Da) or two molecules of 9-*cis*-retinoic acid (300 Da). The lower portion of the cavity projects from the heme iron toward the open entrance to the active site on the N-terminal side of the B-C loop under helix F′. This arm is occupied by one retinoic acid molecule, with its carboxylate in the entrance channel and the trimethylcyclohexenyl ring positioned for hydroxylation. The distal molecule is stacked above the proximal molecule, with the carboxylate in a second entrance on the C-terminal side of the B-C loop, where it forms an ionic bond with Arg-241 on helix G, and its trimethylcyclohexenyl ring is stacked above the midpoint of the proximal retinoic acid. The two arms of the cavity complement the shape of montelukast, which exhibits three large groups attached to a chiral carbon (Fig. 1). In contrast, felodipine (384 Da) and troglitazone (442 Da) occupy only a portion of the cavity (77). The structure of the enzyme crystallized in the absence of a ligand (78) does not differ greatly from that of the ligand complexes (77). This apparent rigidity could reflect the presence of a fatty acid bound to the exterior surface of 2C8, with the aliphatic chain passing through the turn formed by helices F′, G′, and G. The location of this peripheral binding site is close to that observed for progesterone in the structure of 3A4.

2C19 plays an important role in the clearance of omeprazole (345 Da) and in the conversion of clopidogrel (322 Da) to its therapeutic metabolite. The backbone conformation of 2C19 complexed with the inhibitor (2-methyl-1-benzofuran-3-yl)-(4-hydroxy-3,5-dimethylphenyl)methanone is highly similar to that of 2C8, but the cavity is divided into a smaller active site and an antechamber under helix F′, which is likely to be part of the substrate access channel. These differences between 2C8 and 2C19 arise from extensive divergence in the amino acid side chains that form the cavities of the two enzymes (79). The separation of the two cavities in 2C19 reflects a constriction formed by the close approach of phenylalanines on the B-C loop and in the turn of the C-terminal loop as seen for 2D6 (Protein Data Bank code 3QM4) (Fig. 3*A*). This antechamber is not evident in P450s 1A, 1B, 2A, and 2E because this region is filled by larger amino side chains.

Similarly, the antechamber is reduced in volume in rabbit 2C5 because the differences in the conformation of the F-F′ loop fill this space as they do in family 1 P450s (Fig. 1) and in the substrate-free 2D6 structure (Protein Data Bank code 2F9Q) (Fig. 3). Nevertheless, the corresponding phenylalanines exhibit significant rotamer differences as well as changes in the F-G region, the C-terminal loop, and the B-C loop when different substrates are bound (80, 81).

Although 2C9 exhibits >90% sequence identity to 2C19, the two enzymes make unique contributions to human drug metabolism. 2C9 contributes extensively to the clearance of small anionic compounds, and 2C9 genetic variation increases risks for adverse effects of warfarin and phenytoin therapies. The functional differences between 2C9 and 2C19 arise from conformational differences due to amino acid differences that reside outside the active site cavity but influence the architecture of the 2C9 active site (79). The alternative conformation of the 2C9 B-C loop positions the conserved Arg-108 in the active site, where it forms an ionic bond with the carboxylate of flurbiprofen in the 2C9 structure (Protein Data Bank code 1R9O). This rearrangement alters both the polar properties and the shape of the active site cavity and underlies the role of 2C9 in the metabolic clearance of other small anionic drugs and the

[2] The abbreviation used is: NNK, nicotine-derived nitrosamine ketone.

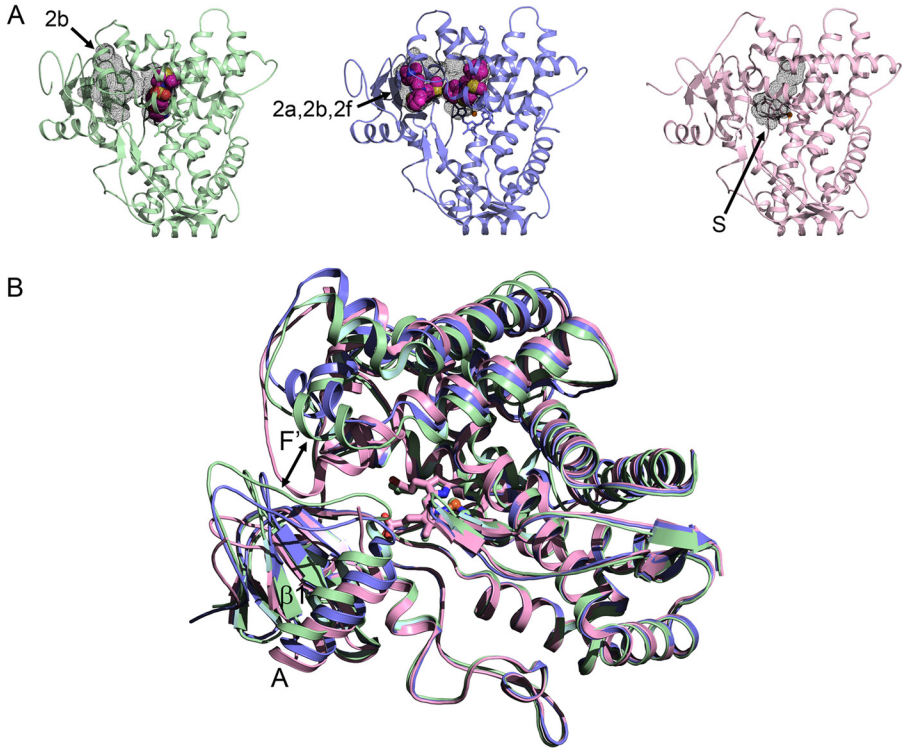

FIGURE 3. **Alternative conformations of microsomal 2D6.** *A*, the 3QM4 structure of 2D6 with prinomastat bound (*green*) exhibits a closed active site cavity and an antechamber (*black mesh* surfaces) with an open 2b channel (*arrow*). The 3TBG structure of 2D6 with two molecules of thioridazine bound (*slate*) displays a single open cavity with merged 2a, 2b, and 2f channels. The 2F9Q structure of 2D6 (*pink*) exhibits an open S channel. *B*, a side view of the overlaid structures shows how conformational changes open the entrance channel in the 3TBG structure relative to the 3QM4 structure (*double-headed arrow*), whereas the F-G loop fills the channel entrance in the 2F9Q structure.

distinct contributions of the two enzymes to drug metabolism (79, 82).

Two additional 2C9 structures (Protein Data Bank codes 1OG2 and 1OG5) determined for a construct with seven amino acid substitutions in the helix F-G region to facilitate crystallization (83) exhibit much larger active site cavities than seen for 2C9 (code 1R9O) (82) or for 2C19 (79). This difference reflects an elevation of the helix F-G region above the heme, a repositioning of the turn in the C-terminal loop away from helix I, and an alternative conformation of the helix B-C loop that places Arg-108 outside the active site in the 1OG2 and 1OG5 structures. *S*-Warfarin (308 Da) is bound in a distal portion of the 1OG5 structure of the 2C9 mutant, which was speculated to serve as an effector site or possibly initial binding site (83). This location corresponds to the antechamber seen in 2C19, and the warfarin-binding site could reflect an initial binding site in the entry way. A similar antechamber binds a second substrate molecule in the structure of 21A2 (41). Similarly, one of two molecules of NNK (207 Da) occupies a similar position in an expanded 2A13 active site, with the other NNK positioned near the heme (56). In contrast, a 2A13 structure for an alternative crystal form exhibits one molecule of NNK positioned for metabolite formation in a small active site for six of eight molecules in the asymmetric unit. Interestingly, one of the two remaining 2A13 molecules of the asymmetric unit exhibits an open access channel under helix F and between the C-terminal loop and helix I (56). This channel is also open in the 2F9Q structure of 2D6 (Fig. 3*A*) crystallized in the absence of a ligand (84).

In contrast, the 3QM4 structure of 2D6 complexed with prinomastat (423 Da) exhibits a closed active site cavity that conforms closely to the size of prinomastat (85). Additionally, an antechamber is evident in the structure of the prinomastat complex below helix F′, similar to that seen in 2C19 (79) and 21A2 (41). There is a significant difference in the conformation of the helix F-G region and neighboring portions of the two structures, and the antechamber is filled in the 2F9Q structure of 2D6 due to the alternative conformation of the helix F-G region (Fig. 3*B*).

A second open structure of 2D6 (Protein Data Bank code 3TBG) was crystallized with thioridazine (371 Da) in the active site, where it forms an ionic bond with Asp-301 on helix I. Many substrates and inhibitors of P450 2D6 have basic nitrogens that are positively charged at neutral pH and that are thought to bind to either Asp-301 or Glu-216 in the active site (86). A second thioridazine is bound in the antechamber of the 3TBG structure. The constriction between the active site cavity and the antechamber of the 3QM4 structure is relaxed to form a continuous channel encompassing the two thioridazine molecules that extends from the active site to the open entrance between the helix F′ and the helix A′ regions in the 3TBG structure (Fig. 3*A*). The thioridazine in the entrance channel forms an ionic bond with Glu-222 on helix F′, suggesting that Glu-222 could facilitate the initial binding of cationic substrates to 2D6. Although binding of a second molecule in the entrance channel could act as an effector, biochemical evidence to support this notion has not been reported for 2D6 with thioridazine, 2A13 with NNK, or 21A2 with 17α-hydroxyprogesterone at enzyme

and substrate concentrations used to assess catalytic activity or ligand binding, which are much lower than those used for crystallization.

The structural flexibility required for opening and closing the cavity can also enable the binding of larger inhibitors or alternative substrates in more open structural conformations. This has been studied extensively in rabbit 2B4, which was first crystallized in an open ligand-free form (87) and subsequently in closed structures with 4-(4-chlorophenyl)imidazole (179 Da) (88) and 1-(4-chlorophenyl)imidazole (179 Da) (89) bound in a small active site cavity. A structure of human 2B6 exhibits a remarkably similar active site when crystallized with 4-(4-chlorophenyl)imidazole (90). Additionally, ticlopidine (264 Da) and clopidogrel (322 Da) complexes of 2B4 exhibit compact closed structures (91), and more recently, ligand-free 2B4 was crystallized in a closed conformation (92). Similarly, complexes of 2B6 with 4-benzylpyridine (169 Da) and 4-(4-nitrobenzyl)pyridine (214 Da) are closed, and this is accompanied by small adaptations (93). Systematic use of azole ligands of increasing size with 2B4, 1-biphenyl-4-methyl-1*H*-imidazole (234 Da) (94) and bifonazole (310 Da) (95), produced a continuum of structures from small and closed to larger and more open active site cavities (96). 2B6 and 2B4 have also been crystallized with two molecules of amlodipine (409 Da) in an expanded active site channel (97).

Additionally, structures have been determined for covalent adducts of 2B4 with reactive metabolites of the irreversible inhibitors 9-ethynylphenanthrene (202 Da) (98) and *tert*-butylphenylacetylene (176 Da) (99) covalently linked to Thr-302 by an ester bond. The latter was crystallized in both the closed and open conformations. An alternative rotamer of the adducted residue opens the active site sufficiently to allow access of other substrates and may underlie the residual activity of the enzyme following adduction. Similarly, double occupancy of open conformations of P450s could underlie substrate-dependent differences in K_i values observed for drug-drug interactions.

Perspective

Structures determined for specialist P450s reveal adaptations that underlie their unique physiologic roles, which require precise positioning of the substrate to produce the appropriate product. It is likely that structural characterization of human P450s will be extended to include P450s in other physiologic pathways as well as P450s targeted for prodrug activation in tumors. Additionally, structural characterization of membrane P450s in other species, including plants and insects, would increase our understanding of the mechanisms of resistance to pesticides and herbicides, and structures of critical P450s in eukaryotic microbial pathogens could facilitate drug design targeting these organisms. Structures determined for several generalist P450s indicate that conformational dynamics contributes to binding diverse ligands. Specialist P450s are also structurally dynamic, as they must open and close for substrate access and product egress. Their physiologic substrates form strong interactions that reduce protein dynamics and increase catalytic specificity and efficiency. The fit of adopted substrates with generalist P450s is less exacting and likely leads to a greater range of substrate and protein dynamics with associated reductions of catalytic efficiencies and metabolic specificities. Characterization of conformational changes that occur when substrates and inhibitors bind is likely to be extended to additional generalist P450s, which will contribute to better *in silico* approaches for understanding structure-activity relationships that aid drug design. Additionally, advances in the application of NMR spectroscopy for structural characterization of membrane P450s could increase our understanding of the conformational heterogeneity of membrane-bound P450s.

REFERENCES

1. Nelson, D. R., Zeldin, D. C., Hoffman, S. M., Maltais, L. J., Wain, H. M., and Nebert, D. W. (2004) Comparison of cytochrome P450 (*CYP*) genes from the mouse and human genomes, including nomenclature recommendations for genes, pseudogenes and alternative-splice variants. *Pharmacogenetics* **14,** 1–18
2. Thomas, J. H. (2007) Rapid birth-death evolution specific to xenobiotic cytochrome P450 genes in vertebrates. *PLoS Genet.* **3,** e67
3. Williams, P. A., Cosme, J., Sridhar, V., Johnson, E. F., and McRee, D. E. (2000) The crystallographic structure of a mammalian microsomal cytochrome P450 monooxygenase: structural adaptations for membrane binding and functional diversity. *Mol. Cell* **5,** 121–131
4. Poulos, T. L., Finzel, B. C., Gunsalus, I. C., Wagner, G. C., and Kraut, J. (1985) The 2.6-Å crystal structure of the *Pseudomonas putida* cytochrome P-450. *J. Biol. Chem.* **260,** 16122–16130
5. Poulos, T. L., and Johnson, E. F. (2005) Structures of cytochrome P450 enzymes. In *Cytochrome P450: Structure, Mechanism, and Biochemistry* (Ortiz de Montellano, P. R., ed) 3rd Ed., pp. 87–114, Kluwer Academic/Plenum Publishers, New York
6. Sirim, D., Widmann, M., Wagner, F., and Pleiss, J. (2010) Prediction and analysis of the modular structure of cytochrome P450 monooxygenases. *BMC Struct. Biol.* **10,** 34
7. Rittle, J., and Green, M. T. (2010) Cytochrome P450 compound I: capture, characterization, and C-H bond activation kinetics. *Science* **330,** 933–937
8. Bridges, A., Gruenke, L., Chang, Y. T., Vakser, I. A., Loew, G., and Waskell, L. (1998) Identification of the binding site on cytochrome P450 2B4 for cytochrome b_5 and cytochrome P450 reductase. *J. Biol. Chem.* **273,** 17036–17049
9. Sevrioukova, I. F., Li, H., Zhang, H., Peterson, J. A., and Poulos, T. L. (1999) Structure of a cytochrome P450-redox partner electron-transfer complex. *Proc. Natl. Acad. Sci. U.S.A.* **96,** 1863–1868
10. Strushkevich, N., MacKenzie, F., Cherkesova, T., Grabovec, I., Usanov, S., and Park, H. W. (2011) Structural basis for pregnenolone biosynthesis by the mitochondrial monooxygenase system. *Proc. Natl. Acad. Sci. U.S.A.* **108,** 10139–10143
11. Zhang, W., Pochapsky, S. S., Pochapsky, T. C., and Jain, N. U. (2008) Solution NMR structure of putidaredoxin-cytochrome P450cam complex via a combined residual dipolar coupling-spin labeling approach suggests a role for Trp106 of putidaredoxin in complex formation. *J. Mol. Biol.* **384,** 349–363
12. Ewen, K. M., Kleser, M., and Bernhardt, R. (2011) Adrenodoxin: the archetype of vertebrate-type [2Fe-2S] cluster ferredoxins. *Biochim. Biophys. Acta* **1814,** 111–125
13. Wang, M., Roberts, D. L., Paschke, R., Shea, T. M., Masters, B. S. S., and Kim, J. J. P. (1997) Three-dimensional structure of NADPH-cytochrome P450 reductase: prototype for FMN- and FAD-containing enzymes. *Proc. Natl. Acad. Sci. U.S.A.* **94,** 8411–8416
14. Xia, C., Hamdane, D., Shen, A. L., Choi, V., Kasper, C. B., Pearl, N. M., Zhang, H., Im, S. C., Waskell, L., and Kim, J. J. (2011) Conformational changes of NADPH-cytochrome P450 oxidoreductase are essential for catalysis and cofactor binding. *J. Biol. Chem.* **286,** 16246–16260
15. Hamdane, D., Xia, C., Im, S. C., Zhang, H., Kim, J. J., and Waskell, L. (2009) Structure and function of an NADPH-cytochrome P450 oxidoreductase in an open conformation capable of reducing cytochrome P450. *J. Biol. Chem.* **284,** 11374–11384
16. Im, S. C., and Waskell, L. (2011) The interaction of microsomal cyto-

chrome P450 2B4 with its redox partners, cytochrome P450 reductase and cytochrome b_5. *Arch. Biochem. Biophys.* **507,** 144–153
17. Ravichandran, K. G., Boddupalli, S. S., Hasermann, C. A., Peterson, J. A., and Deisenhofer, J. (1993) Crystal structure of hemoprotein domain of P450BM-3, a prototype for microsomal P450s. *Science* **261,** 731–736
18. Li, H., and Poulos, T. L. (1997) The structure of the cytochrome P450BM-3 haem domain complexed with the fatty acid substrate, palmitoleic acid. *Nat. Struct. Biol.* **4,** 140–146
19. Cojocaru, V., Winn, P. J., and Wade, R. C. (2007) The ins and outs of cytochrome P450s. *Biochim. Biophys. Acta* **1770,** 390–401
20. Black, S. D. (1992) Membrane topology of the mammalian P450 cytochromes. *FASEB J.* **6,** 680–685
21. Ghosh, D., Griswold, J., Erman, M., and Pangborn, W. (2010) X-ray structure of human aromatase reveals an androgen-specific active site. *J. Steroid Biochem. Mol. Biol.* **118,** 197–202
22. Cosme, J., and Johnson, E. F. (2000) Engineering microsomal cytochrome P450 2C5 to be a soluble, monomeric enzyme. Mutations that alter aggregation, phospholipid dependence of catalysis, and membrane binding. *J. Biol. Chem.* **275,** 2545–2553
23. Von Wachenfeldt, C., and Johnson, E. F. (1995) Structures of eukaryotic cytochrome P450 enzymes. In *Cytochrome P450: Structure, Mechanism, and Biochemistry* (Ortiz de Montellano, P. R., ed) 2nd Ed., pp. 183–223, Plenum Press, New York
24. Ozalp, C., Szczesna-Skorupa, E., and Kemper, B. (2006) Identification of membrane-contacting loops of the catalytic domain of cytochrome P450 2C2 by tryptophan fluorescence scanning. *Biochemistry* **45,** 4629–4637
25. Mast, N., Liao, W. L., Pikuleva, I. A., and Turko, I. V. (2009) Combined use of mass spectrometry and heterologous expression for identification of membrane-interacting peptides in cytochrome P450 46A1 and NADPH-cytochrome P450 oxidoreductase. *Arch. Biochem. Biophys.* **483,** 81–89
26. Denisov, I. G., Shih, A. Y., and Sligar, S. G. (2012) Structural differences between soluble and membrane bound cytochrome P450s. *J. Inorg. Biochem.* **108,** 150–158
27. DuBois, R. N., Simpson, E. R., Tuckey, J., Lambeth, J. D., and Waterman, M. R. (1981) Evidence for a higher molecular weight precursor of cholesterol side chain cleavage cytochrome P-450 and induction of mitochondrial and cytosolic proteins by corticotropin in adult bovine adrenal cells. *Proc. Natl. Acad. Sci. U.S.A.* **78,** 1028–1032
28. Nabi, N., Kominami, S., Takemori, S., and Omura, T. (1980) *In vitro* synthesis of mitochondrial cytochromes P-450(scc) and P-450 (11-β) and microsomal cytochrome P-450(C-21) by both free and bound polysomes isolated from bovine adrenal cortex. *Biochem. Biophys. Res. Commun.* **97,** 687–693
29. Headlam, M. J., Wilce, M. C., and Tuckey, R. C. (2003) The F-G loop region of cytochrome P450scc (CYP11A1) interacts with the phospholipid membrane. *Biochim. Biophys. Acta* **1617,** 96–108
30. Annalora, A. J., Goodin, D. B., Hong, W. X., Zhang, Q., Johnson, E. F., and Stout, C. D. (2010) The crystal structure of CYP24A1, a mitochondrial cytochrome P450 involved in vitamin D metabolism. *J. Mol. Biol.* **396,** 441–451
31. Berka, K., Hendrychová, T., Anzenbacher, P., and Otyepka, M. (2011) Membrane position of ibuprofen agrees with suggested access path entrance to cytochrome P450 2C9 active site. *J. Phys. Chem. A* **115,** 11248–11255
32. Cojocaru, V., Balali-Mood, K., Sansom, M. S., and Wade, R. C. (2011) Structure and dynamics of the membrane-bound cytochrome P450 2C9. *PLoS Comput. Biol.* **7,** e1002152
33. Mast, N., Annalora, A. J., Lodowski, D. T., Palczewski, K., Stout, C. D., and Pikuleva, I. A. (2011) Structural basis for three-step sequential catalysis by the cholesterol side chain cleavage enzyme CYP11A1. *J. Biol. Chem.* **286,** 5607–5613
34. Mast, N., White, M. A., Bjorkhem, I., Johnson, E. F., Stout, C. D., and Pikuleva, I. A. (2008) Crystal structures of substrate-bound and substrate-free cytochrome P450 46A1, the principal cholesterol hydroxylase in the brain. *Proc. Natl. Acad. Sci. U.S.A.* **105,** 9546–9551
35. Mast, N., Linger, M., Clark, M., Wiseman, J., Stout, C. D., and Pikuleva, I. A. (2012) *In silico* and intuitive predictions of CYP46A1 inhibition by marketed drugs with subsequent enzyme crystallization in complex with fluvoxamine. *Mol. Pharmacol.* **82,** 824–834
36. Mast, N., Charvet, C., Pikuleva, I. A., and Stout, C. D. (2010) Structural basis of drug binding to CYP46A1, an enzyme that controls cholesterol turnover in the brain. *J. Biol. Chem.* **285,** 31783–31795
37. Strushkevich, N., Usanov, S. A., Plotnikov, A. N., Jones, G., and Park, H. W. (2008) Structural analysis of CYP2R1 in complex with vitamin D_3. *J. Mol. Biol.* **380,** 95–106
38. Akhtar, M., Wright, J. N., and Lee-Robichaud, P. (2011) A review of mechanistic studies on aromatase (CYP19) and 17α-hydroxylase-17,20-lyase (CYP17). *J. Steroid Biochem. Mol. Biol.* **125,** 2–12
39. Ghosh, D., Lo, J., Morton, D., Valette, D., Xi, J., Griswold, J., Hubbell, S., Egbuta, C., Jiang, W., An, J., and Davies, H. M. (2012) Novel aromatase inhibitors by structure-guided design. *J. Med. Chem.* **55,** 8464–8476
40. DeVore, N. M., and Scott, E. E. (2012) Structures of cytochrome P450 17A1 with prostate cancer drugs abiraterone and TOK-001. *Nature* **482,** 116–119
41. Zhao, B., Lei, L., Kagawa, N., Sundaramoorthy, M., Banerjee, S., Nagy, L. D., Guengerich, F. P., and Waterman, M. R. (2012) Three-dimensional structure of steroid 21-hydroxylase (cytochrome P450 21A2) with two substrates reveals locations of disease-associated variants. *J. Biol. Chem.* **287,** 10613–10622
42. Strushkevich, N., Gilep, A. A., Shen, L., Arrowsmith, C. H., Edwards, A. M., Usanov, S. A., and Park, H. W. (2013) Structural insights into aldosterone synthase substrate specificity and targeted inhibition. *Mol. Endocrinol.* **27,** 315–324
43. Strushkevich, N., Usanov, S. A., and Park, H. W. (2010) Structural basis of human CYP51 inhibition by antifungal azoles. *J. Mol. Biol.* **397,** 1067–1078
44. Lepesheva, G. I., Park, H. W., Hargrove, T. Y., Vanhollebeke, B., Wawrzak, Z., Harp, J. M., Sundaramoorthy, M., Nes, W. D., Pays, E., Chaudhuri, M., Villalta, F., and Waterman, M. R. (2010) Crystal structures of *Trypanosoma brucei* sterol 14α-demethylase and implications for selective treatment of human infections. *J. Biol. Chem.* **285,** 1773–1780
45. Hargrove, T. Y., Wawrzak, Z., Liu, J., Waterman, M. R., Nes, W. D., and Lepesheva, G. I. (2012) Structural complex of sterol 14α-demethylase (CYP51) with 14α-methylenecyclopropyl-Δ7–24,25-dihydrolanosterol. *J. Lipid Res.* **53,** 311–320
46. Lepesheva, G. I., Hargrove, T. Y., Anderson, S., Kleshchenko, Y., Furtak, V., Wawrzak, Z., Villalta, F., and Waterman, M. R. (2010) Structural insights into inhibition of sterol 14α-demethylase in the human pathogen *Trypanosoma cruzi*. *J. Biol. Chem.* **285,** 25582–25590
47. Chiang, C. W., Yeh, H. C., Wang, L. H., and Chan, N. L. (2006) Crystal structure of the human prostacyclin synthase. *J. Mol. Biol.* **364,** 266–274
48. Li, Y. C., Chiang, C. W., Yeh, H. C., Hsu, P. Y., Whitby, F. G., Wang, L. H., and Chan, N. L. (2008) Structures of prostacyclin synthase and its complexes with substrate-analog and inhibitor reveal a ligand-specific heme conformation change. *J. Biol. Chem.* **283,** 2917–2926
49. Hecker, M., and Ullrich, V. (1989) On the mechanism of prostacyclin and thromboxane A_2 biosynthesis. *J. Biol. Chem.* **264,** 141–150
50. Lee, D. S., Nioche, P., Hamberg, M., and Raman, C. S. (2008) Structural insights into the evolutionary paths of oxylipin biosynthetic enzymes. *Nature* **455,** 363–368
51. Rendic, S., and Guengerich, F. P. (2012) Contributions of human enzymes in carcinogen metabolism. *Chem. Res. Toxicol.* **25,** 1316–1383
52. Sansen, S., Yano, J. K., Reynald, R. L., Schoch, G. A., Griffin, K. J., Stout, C. D., and Johnson, E. F. (2007) Adaptations for the oxidation of polycyclic aromatic hydrocarbons exhibited by the structure of human P450 1A2. *J. Biol. Chem.* **282,** 14348–14355
53. Wang, A., Savas, U., Stout, C. D., and Johnson, E. F. (2011) Structural characterization of the complex between α-naphthoflavone and human cytochrome P450 1B1. *J. Biol. Chem.* **286,** 5736–5743
54. Gotoh, O. (1992) Substrate recognition sites in cytochrome P450 family 2 (CYP2) proteins inferred from comparative analyses of amino acid and coding nucleotide sequences. *J. Biol. Chem.* **267,** 83–90
55. Yano, J. K., Hsu, M. H., Griffin, K. J., Stout, C. D., and Johnson, E. F. (2005) Structures of human microsomal cytochrome P450 2A6 complexed with coumarin and methoxsalen. *Nat. Struct. Mol. Biol.* **12,** 822–823
56. DeVore, N. M., and Scott, E. E. (2012) Nicotine and 4-(methylnitro-

samino)-1-(3-pyridyl)-1-butanone binding and access channel in human cytochrome P450 2A6 and 2A13 enzymes. *J. Biol. Chem.* **287,** 26576–26585
57. Yano, J. K., Denton, T. T., Cerny, M. A., Zhang, X., Johnson, E. F., and Cashman, J. R. (2006) Synthetic inhibitors of cytochrome P-450 2A6: inhibitory activity, difference spectra, mechanism of inhibition, and protein cocrystallization. *J. Med. Chem.* **49,** 6987–7001
58. Smith, B. D., Sanders, J. L., Porubsky, P. R., Lushington, G. H., Stout, C. D., and Scott, E. E. (2007) Structure of the human lung cytochrome P450 2A13. *J. Biol. Chem.* **282,** 17306–17313
59. Porubsky, P. R., Meneely, K. M., and Scott, E. E. (2008) Structures of human cytochrome P450 2E1. Insights into the binding of inhibitors and both small molecular weight and fatty acid substrates. *J. Biol. Chem.* **283,** 33698–33707
60. Porubsky, P. R., Battaile, K. P., and Scott, E. E. (2010) Human cytochrome P450 2E1 structures with fatty acid analogs reveal a previously unobserved binding mode. *J. Biol. Chem.* **285,** 22282–22290
61. DeVore, N. M., Meneely, K. M., Bart, A. G., Stephens, E. S., Battaile, K. P., and Scott, E. E. (2012) Structural comparison of cytochromes P450 2A6, 2A13, and 2E1 with pilocarpine. *FEBS J.* **279,** 1621–1631
62. Cruciani, G., Carosati, E., De Boeck, B., Ethirajulu, K., Mackie, C., Howe, T., and Vianello, R. (2005) MetaSite: understanding metabolism in human cytochromes from the perspective of the chemist. *J. Med. Chem.* **48,** 6970–6979
63. de Groot, M. J. (2006) Designing better drugs: predicting cytochrome P450 metabolism. *Drug Discov. Today* **11,** 601–606
64. Sun, H., and Scott, D. O. (2010) Structure-based drug metabolism predictions for drug design. *Chem. Biol. Drug Des.* **75,** 3–17
65. Kirchmair, J., Williamson, M. J., Tyzack, J. D., Tan, L., Bond, P. J., Bender, A., and Glen, R. C. (2012) Computational prediction of metabolism: sites, products, SAR, P450 enzyme dynamics, and mechanisms. *J. Chem. Inf. Model.* **52,** 617–648
66. Zanger, U. M., Turpeinen, M., Klein, K., and Schwab, M. (2008) Functional pharmacogenetics/genomics of human cytochromes P450 involved in drug biotransformation. *Anal. Bioanal. Chem.* **392,** 1093–1108
67. Yano, J. K., Wester, M. R., Schoch, G. A., Griffin, K. J., Stout, C. D., and Johnson, E. F. (2004) The structure of human microsomal cytochrome P450 3A4 determined by x-ray crystallography to 2.05-Å resolution. *J. Biol. Chem.* **279,** 38091–38094
68. Williams, P. A., Cosme, J., Vinkovic, D. M., Ward, A., Angove, H. C., Day, P. J., Vonrhein, C., Tickle, I. J., and Jhoti, H. (2004) Crystal structures of human cytochrome P450 3A4 bound to metyrapone and progesterone. *Science* **305,** 683–686
69. Ekroos, M., and Sjögren, T. (2006) Structural basis for ligand promiscuity in cytochrome P450 3A4. *Proc. Natl. Acad. Sci. U.S.A.* **103,** 13682–13687
70. Sevrioukova, I. F., and Poulos, T. L. (2010) Structure and mechanism of the complex between cytochrome P4503A4 and ritonavir. *Proc. Natl. Acad. Sci. U.S.A.* **107,** 18422–18427
71. Sevrioukova, I. F., and Poulos, T. L. (2012) Interaction of human cytochrome P4503A4 with ritonavir analogs. *Arch. Biochem. Biophys.* **520,** 108–116
72. Sevrioukova, I. F., and Poulos, T. L. (2012) Structural and mechanistic insights into the interaction of cytochrome P4503A4 with bromoergocryptine, a type I ligand. *J. Biol. Chem.* **287,** 3510–3517
73. Isin, E. M., and Guengerich, F. P. (2008) Substrate binding to cytochromes P450. *Anal Bioanal. Chem.* **392,** 1019–1030
74. Denisov, I. G., and Sligar, S. G. (2012) A novel type of allosteric regulation: functional cooperativity in monomeric proteins. *Arch. Biochem. Biophys.* **519,** 91–102
75. Roberts, A. G., Yang, J., Halpert, J. R., Nelson, S. D., Thummel, K. T., and Atkins, W. M. (2011) The structural basis for homotropic and heterotropic cooperativity of midazolam metabolism by human cytochrome P450 3A4. *Biochemistry* **50,** 10804–10818
76. Davydov, D. R., Rumfeldt, J. A., Sineva, E. V., Fernando, H., Davydova, N. Y., and Halpert, J. R. (2012) Peripheral ligand-binding site in cytochrome P450 3A4 located with fluorescence resonance energy transfer (FRET). *J. Biol. Chem.* **287,** 6797–6809
77. Schoch, G. A., Yano, J. K., Sansen, S., Dansette, P. M., Stout, C. D., and Johnson, E. F. (2008) Determinants of cytochrome P450 2C8 substrate binding. Structures of complexes with montelukast, troglitazone, felodipine, and 9-*cis*-retinoic acid. *J. Biol. Chem.* **283,** 17227–17237
78. Schoch, G. A., Yano, J. K., Wester, M. R., Griffin, K. J., Stout, C. D., and Johnson, E. F. (2004) Structure of human microsomal cytochrome P450 2C8. Evidence for a peripheral fatty acid binding site. *J. Biol. Chem.* **279,** 9497–9503
79. Reynald, R. L., Sansen, S., Stout, C. D., and Johnson, E. F. (2012) Structural characterization of human cytochrome P450 2C19. Active site differences between P450s 2C8, 2C9, and 2C19. *J. Biol. Chem.* **287,** 44581–44591
80. Wester, M. R., Johnson, E. F., Marques-Soares, C., Dansette, P. M., Mansuy, D., and Stout, C. D. (2003) The structure of a substrate complex of mammalian cytochrome P450 2C5 at 2.3 Å resolution: evidence for multiple substrate binding modes. *Biochemistry* **42,** 6370–6379
81. Wester, M. R., Johnson, E. F., Marques-Soares, C., Dijols, S., Dansette, P. M., Mansuy, D., and Stout, C. D. (2003) The structure of mammalian cytochrome P450 2C5 complexed with diclofenac at 2.1 Å resolution: evidence for an induced fit model of substrate binding. *Biochemistry* **42,** 9335–9345
82. Wester, M. R., Yano, J. K., Schoch, G. A., Yang, C., Griffin, K. J., Stout, C. D., and Johnson, E. F. (2004) The structure of human microsomal cytochrome P450 2C9 complexed with flurbiprofen at 2.0 Å resolution. *J. Biol. Chem.* **279,** 35630–35637
83. Williams, P. A., Cosme, J., Ward, A., Angove, H. C., Matak Vinković, D., and Jhoti, H. (2003) Crystal structure of human cytochrome P450 2C9 with bound warfarin. *Nature* **424,** 464–468
84. Rowland, P., Blaney, F. E., Smyth, M. G., Jones, J. J., Leydon, V. R., Oxbrow, A. K., Lewis, C. J., Tennant, M. G., Modi, S., Eggleston, D. S., Chenery, R. J., and Bridges, A. M. (2006) Crystal structure of human cytochrome P450 2D6. *J. Biol. Chem.* **281,** 7614–7622
85. Wang, A., Savas, U., Hsu, M. H., Stout, C. D., and Johnson, E. F. (2012) Crystal structure of human cytochrome P450 2D6 with prinomastat bound. *J. Biol. Chem.* **287,** 10834–10843
86. Wang, B., Yang, L. P., Zhang, X. Z., Huang, S. Q., Bartlam, M., and Zhou, S. F. (2009) New insights into the structural characteristics and functional relevance of the human cytochrome P450 2D6 enzyme. *Drug Metab. Rev.* **41,** 573–643
87. Scott, E. E., He, Y. A., Wester, M. R., White, M. A., Chin, C. C., Halpert, J. R., Johnson, E. F., and Stout, C. D. (2003) An open conformation of mammalian cytochrome P450 2B4 at 1.6-Å resolution. *Proc. Natl. Acad. Sci. U.S.A.* **100,** 13196–13201
88. Scott, E. E., White, M. A., He, Y. A., Johnson, E. F., Stout, C. D., and Halpert, J. R. (2004) Structure of mammalian cytochrome P450 2B4 complexed with 4-(4-chlorophenyl)imidazole at 1.9 Å resolution. Insight into the range of P450 conformations and coordination of redox partner binding. *J. Biol. Chem.* **279,** 27294–27301
89. Zhao, Y., Sun, L., Muralidhara, B. K., Kumar, S., White, M. A., Stout, C. D., and Halpert, J. R. (2007) Structural and thermodynamic consequences of 1-(4-chlorophenyl)imidazole binding to cytochrome P450 2B4. *Biochemistry* **46,** 11559–11567
90. Gay, S. C., Shah, M. B., Talakad, J. C., Maekawa, K., Roberts, A. G., Wilderman, P. R., Sun, L., Yang, J. Y., Huelga, S. C., Hong, W. X., Zhang, Q., Stout, C. D., and Halpert, J. R. (2010) Crystal structure of a cytochrome P450 2B6 genetic variant in complex with the inhibitor 4-(4-chlorophenyl)imidazole at 2.0-Å resolution. *Mol. Pharmacol.* **77,** 529–538
91. Gay, S. C., Roberts, A. G., Maekawa, K., Talakad, J. C., Hong, W. X., Zhang, Q., Stout, C. D., and Halpert, J. R. (2010) Structures of cytochrome P450 2B4 complexed with the antiplatelet drugs ticlopidine and clopidogrel. *Biochemistry* **49,** 8709–8720
92. Wilderman, P. R., Shah, M. B., Liu, T., Li, S., Hsu, S., Roberts, A. G., Goodlett, D. R., Zhang, Q., Woods, V. L., Jr., Stout, C. D., and Halpert, J. R. (2010) Plasticity of cytochrome P450 2B4 as investigated by hydrogen-deuterium exchange mass spectrometry and x-ray crystallography. *J. Biol. Chem.* **285,** 38602–38611
93. Shah, M. B., Pascual, J., Zhang, Q., Stout, C. D., and Halpert, J. R. (2011) Structures of cytochrome P450 2B6 bound to 4-benzylpyridine and 4-(4-nitrobenzyl)pyridine: insight into inhibitor binding and rearrangement of active site side chains. *Mol. Pharmacol.* **80,** 1047–1055

94. Gay, S. C., Sun, L., Maekawa, K., Halpert, J. R., and Stout, C. D. (2009) Crystal structures of cytochrome P450 2B4 in complex with the inhibitor 1-biphenyl-4-methyl-1*H*-imidazole: ligand-induced structural response through α-helical repositioning. *Biochemistry* **48,** 4762–4771
95. Zhao, Y., White, M. A., Muralidhara, B. K., Sun, L., Halpert, J. R., and Stout, C. D. (2006) Structure of microsomal cytochrome P450 2B4 complexed with the antifungal drug bifonazole. Insight into P450 conformational plasticity and membrane interaction. *J. Biol. Chem.* **281,** 5973–5981
96. Halpert, J. R. (2011) The 2010 Bernard B. Brodie Award Lecture. Structure and function of cytochromes P450 2B: from mechanism-based inactivators to x-ray crystal structures and back. *Drug Metab. Dispos.* **39,** 1113–1121
97. Shah, M. B., Wilderman, P. R., Pascual, J., Zhang, Q., Stout, C. D., and Halpert, J. R. (2012) Conformational adaptation of human cytochrome P450 2B6 and rabbit cytochrome P450 2B4 revealed upon binding multiple amlodipine molecules. *Biochemistry* **18,** 7225–7238
98. Zhang, H., Gay, S. C., Shah, M., Foroozesh, M., Liu, J., Osawa, Y., Zhang, Q., Stout, C. D., Halpert, J. R., and Hollenberg, P. F. (2013) Potent mechanism-based inactivation of cytochrome P450 2B4 by 9-ethynylphenanthrene: implications for allosteric modulation of cytochrome P450 catalysis. *Biochemistry* **52,** 355–364
99. Gay, S. C., Zhang, H., Wilderman, P. R., Roberts, A. G., Liu, T., Li, S., Lin, H. L., Zhang, Q., Woods, V. L., Jr., Stout, C. D., Hollenberg, P. F., and Halpert, J. R. (2011) Structural analysis of mammalian cytochrome P450 2B4 covalently bound to the mechanism-based inactivator *tert*-butylphenylacetylene: insight into partial enzymatic activity. *Biochemistry* **50,** 4903–4911